JACS
JOURNAL OF THE AMERICAN CHEMICAL SOCIETY
Article
pubs.acs.org/JACS

Size- and Orientation-Selective Si Nanowire Growth: Thermokinetic Effects of Nanoscale Plasma Chemistry

Hamid Mehdipour[†] and Kostya (Ken) Ostrikov*[,†]

Plasma Nanoscience Centre Australia (PNCA), CSIRO Materials Science and Engineering, P.O. Box 218, Lindfield, New South Wales 2070, Australia and Plasma Nanoscience @ Complex Systems, The University of Sydney, New South Wales 2006, Australia

Supporting Information

ABSTRACT: A multiscale, multiphase thermokinetic model is used to show the effective control of the growth orientation of thin Si NWs for nanoelectronic devices enabled by nanoscale plasma chemistry. It is shown that very thin Si NWs with [110] growth direction can nucleate at much lower process temperatures and pressures compared to thermal chemical vapor deposition where [111]-directed Si NWs are predominantly grown. These findings explain a host of experimental results and offer the possibility of energy- and matter-efficient, size- and orientation-controlled growth of [110] Si NWs for next-generation nanodevices.

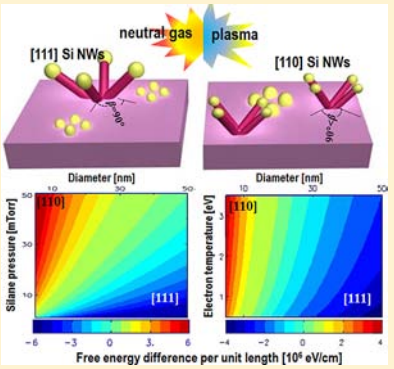

1. INTRODUCTION

Owing to their fascinating semiconducting, chemical, and biocompatibility properties as well as the effective quantum confinement in two dimensions, inorganic NWs (NWs) are exceptional candidates for a variety of applications ranging from field effect transistors (FETs) and lasers to biosensors and energy conversion and storage devices.[1−6] The NW response in nanoscale applications critically depends on their elemental composition, structural, and morphological properties. Despite many years of intense research and a number of established applications of NWs, the problem of effective control of the structural and morphological parameters, such as the NW length, diameter, and the growth direction, still remains unsolved. The as-grown NW networks commonly contain a mix of thick and thin NWs grown along different directions. Therefore, versatile nanoscale synthesis approaches are required to produce sufficiently long NWs with narrowed distributions of diameters and orientations. For example, selective growth of thin Si NWs along [110] direction is highly warranted for next-generation high-speed, high-density FET nanoelectronic devices[3,7,8] at nanodevice-friendly temperatures while maintaining their structural integrity. This approach to thinning Si NWs is quite different compared to oxidizing their outer surfaces (followed by the removal of the outer oxide layer) recently studied using molecular dynamics (MD) simulations.[9]

The [110]-oriented Si NWs have attracted an enormous recent interest as viable building blocks of the future nanoelectronic devices because of the very high hole and electron mobilities, compared to [100] and [111] Si NWs.[8,10−12] These features are required for high-speed FETs with the advanced on-current capability, very low functional response delay,[4] and highly tunable conductance of the quantum tunnel barrier.[7] Also, a much higher figure of merit is expected for [110] NWs because of their large band gap (which increases further as the NWs get thinner)[13] and lower thermal conductivity.[12] A combination of these factors makes the [110]-oriented thin NWs very promising building blocks of the future sensing and nanoelectronic devices.

However, it is very challenging to grow thin Si [110] NWs at low temperatures and pressures using conventional neutral gas-based approaches. In this case, thermal production of building units (BUs) is insufficient while more and more BUs are expelled out as the catalyst nanoparticle (CNP) size decreases.[14] This is why no Si NW nucleation takes place or thicker [111]-oriented Si NWs predominantly nucleate when Au CNPs with a broad size distribution are used.[14] To overcome this adverse effect, the catalyst temperature and the gas pressure have to exceed the critical values,[15] which can be as high as 800 °C[16] and 100 Torr,[17] respectively. However, kinking and other growth defects are frequently observed under high-pressure conditions.[15,18,19] High temperatures, on the other hand, lead to unwanted coalescence of small CNPs and loss of control of the NW size and orientations. Moreover, large amounts of energy and matter are unnecessarily wasted. More advantageous features, applications, and challenges in thermal growth of [110] NWs are summarized in the Supporting Information (SI).

Recent plasma-enhanced chemical vapor deposition (PECVD) experiments showed that even a short low-density plasma exposure leads to the growth of high-density arrays of

Received: November 8, 2012
Published: January 8, 2013

dx.doi.org/10.1021/ja3110279 | J. Am. Chem. Soc. 2013, 135, 1912−1918

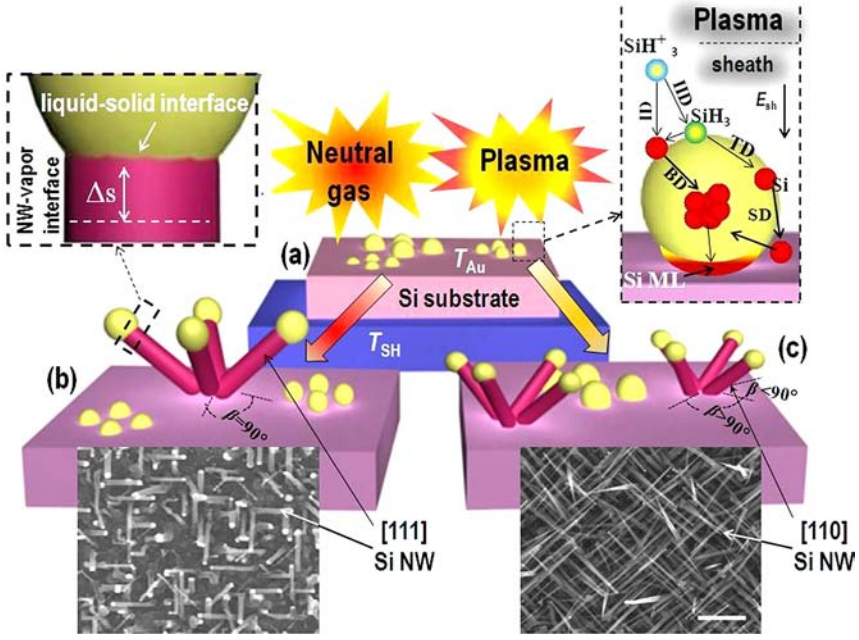

Figure 1. Schematics of the Au catalyst-assisted growth of Si NWs on a Si substrate in Ar + H_2 + SiH_4 neutral gas-/plasma-based CVD. (a) Neutral gas and plasma-enhanced CVD. (b) The growth of [111]-oriented Si NWs under the neutral gas exposure. (c) The growth of the Si NWs along [110] direction using the plasma generation in the same gas mixture. The right magnified view shows the most important surface processes involved in Si atom production and transport channels into/out of the CNPs and stable Si ML nucleation. The associated kinetic processes are thermal dissociation of SiH_4 molecules (TD), ion-induced dissociation (IID), ion decomposition (ID), bulk (BD), and surface (SD) diffusion of Si atoms into the CNP as well as desorption (DE) of the Si atoms out of the CNP. The left magnified view shows the schematics of the liquid−solid interfacial region. SEM images of Si NWs grown on Si (100) substrate via thermal CVD (left) and PECVD (right) by Aella et al.[20] The micrographs are reproduced with permission. Copyright 2007 Wiley-VCH Verlag GmbH & Co. KGaA, Weinheim.

thin Si NWs preferentially oriented along the [110] direction.[20−22] The [110] Si NWs were grown at temperatures and pressures, as low as 250 °C[22] and 50 mTorr, respectively, which are much lower compared to thermal CVD.[17] A similar effect was achieved in the plasma-assisted growth of NWs of other materials.[23−25] Also, plasma-grown Si NWs are usually much thinner than in the equivalent neutral gas-based processes.[20] For example, dense arrays of [110] Si NWs with the average thickness of <20 nm were fabricated in SiH_4 + H_2 plasmas.[20] These experimental results show the possibility of effective plasma-based control of the Si NW size and growth direction. This can be achieved by varying the process pressure and temperature, precursor gas composition, input power, and the plasma treatment time.[20]

This is why a clear understanding of the Si NW growth mechanism in its entirety, including the kinetics of the NW nucleation and growth and thermodynamic selection of the Si NW size and preferential growth orientation as well as the plasma-specific effects, is vitally needed to explain these experimental observations. Previous studies merely used a thermodynamic approach to identify predominant Si NW growth directions.[26] A HRTEM-based study of Ge NW growth[27] clearly showed the importance of the low-energy faceting of a small ML in the Au-catalyzed growth of Ge NWs along the [110] direction. However, it was recently revealed that the NW crystal structure is mostly determined by the growth kinetics rather than thermodynamic factors.[28] Here we use the multiscale, multiphase thermokinetic model to relate the gas-/plasma-specific kinetic effects of the nanoscale reactive chemistry on the surface and within CNPs (i.e., surface processes responsible for Si atom production and transport to the nucleation sites) to the thermodynamic selection rules for the nucleation of the two [111] and [110] most commonly observed orientations of Si NWs. It is shown that these kinetic factors are crucial for the size- and orientation-selective Si NW growth both in thermal and plasma-assisted CVDs.

Our model uniquely combines the plasma-specific, kinetic, and thermodynamic factors to explain the experimentally observed transition from a less important [111] to the highly desired [110] orientation by invoking the nanoscale plasma chemistry effects. The model also confirms the possibility of nucleation of thin Si NWs with the desired orientation even at low temperatures and pressures. This is challenging, if possible at all, through conventional thermal synthesis under the same conditions. The results of our numerical modeling can be used to interpret a host of experimental observations on the thermal and plasma CVD of NWs. In particular, they explain the formation of high-density arrays of thin [110]-oriented Si NWs at lower temperatures and pressures[20−22] compared to equivalent thermal CVD experiments.[17,29] This modeling also provides specific suggestions for the effective control of the NW orientation and the crystalline structure, the critical issues in a very large number of nanoscale chemical synthesis processes.

2. RESULTS AND DISCUSSION

2.1. Nanoscale Plasma Chemistry and Gibbs−Thomson Effect. We consider the Au CNP-assisted nucleation of a Si NW in reactive plasmas of Ar + H_2 + SiH_4 gas mixtures commonly used in plasma-aided synthesis of Si NWs.[20,21] Figure 1 shows the Si NW nucleation on an externally biased Si substrate placed on a holder platform heated externally to temperature T_{SH} (a). It also shows a schematic and the micrographs of [111]- and [110]-oriented Si NWs synthesized in CVD (b) and PECVD (c) experiments, respectively. Also,

dx.doi.org/10.1021/ja3110279 | J. Am. Chem. Soc. 2013, 135, 1912−1918

the most important elementary surface processes are shown in a magnified sketch of the Au CNP (right inset). The detailed description of the model and the main assumptions can be found in the SI. The main step in the Si monolayer (ML) nucleation is the supersaturation of the AuSi alloy in the CNP (see Figure S1). It is assumed that the AuSi alloy catalyst is molten and the Si atom equilibrium concentration is constant in the temperature range considered. More details about the AuSi system can be found in the SI. The nucleation is adversely affected by the Gibbs−Thompson (GT) effect which leads to the expulsion of Si atoms (BUs of the NWs) from the catalyst bulk to the top surface of small CNPs. As the CNP gets smaller or the temperature and pressure decrease, the GT effect becomes stronger and weakens the driving force for the Si ML nucleation.[14] Moreover, less effective thermal generation of Si atoms at low temperatures (due to less effective thermal decomposition of SiH_4 molecules as the only possible Si atom generation process) leads to less effective transport of BUs into the catalyst and thus very low level of the CNP saturation with the BUs. As a result, the formation of a Si ML at the droplet−substrate interface becomes more difficult, and consequently, no Si NW growth takes place, or very large Si MLs are formed over longer time periods. This scenario prevails as long as the level of supersaturation is low due to small number of Si atoms produced and significant outward fluxes of Si stoms.[20] Therefore, when the temperature and pressure are high enough or the catalyst radius is large, the driving force for nucleation of Si MLs increases, which in turn leads to nucleation of stable smaller Si MLs at the catalyst−substrate interface.[14]

In contrast, when the temperature is not high enough, only Si NWs with large diameters can grow or the Si NW nucleation ceases due to the GT effect. It is also known that when the Si NW radius is larger than a critical value, the Si growth proceeds along the direction with the lowest Au liquid−Si ML interfacial energy (the [111] orientation in this work). Otherwise, if the NW thickness is less than the critical diameter or the surface-to-volume ratio increases, the NWs with the lowest surface energies, e.g., the [110]-oriented NWs, are nucleated.[17,18,26,27] This is because at larger diameters the energy of the catalyst−NW interface contributes more than the NW surface energy, whereas at smaller diameters (when the surface-to-volume ratio is high) the NW surface energy determines the thermodynamically favorable orientation.

In this work, we demonstrate that the controlled nanoscale plasma chemistry at the plasma−catalyst interface can provide enough BUs (thus effectively mediate the impact of the GT effect) under low-temperature and low-pressure conditions and lead to size- and orientation-selective nucleation of Si NWs underneath small CNPs at notably lower temperatures and pressures compared to thermal CVD experiments. The impact of the GT effect can be reduced due to effective Si atom generation in the plasma and at the plasma−catalyst interface, controlled transport of species, unique nonthermal, plasma-specific Si atom generation processes, and plasma-induced heating of the catalyst surface.[32] These plasma-related effects in turn lead to the production of sufficient amounts of Si atoms at low temperatures and pressures. This counteracts the reduction of the number of Si atoms in the catalyst and consequently reduces the higher energy barrier induced by the GT effect.[14] In this case, much stronger fluxes of Si atoms into the catalyst and faster supersaturation of the AuSi alloy can be achieved well before coagulation of small catalyst particles becomes significant. This eventually leads to nucleation of Si NWs with the desired thickness and orientation without compromising the CNP size distribution in the prefabricated catalyst patterns. Furthermore, the plasma heating and Si generation mechanisms strongly depend on the plasma parameters. Therefore, it is possible to optimize the plasma parameters to achieve the desired effects in the NW growth control. In this way, the size- and orientation-selective growth of Si NWs can be achieved, as described below.

2.2. Plasma-Assisted Nucleation of Si Monolayer: Low-Temperature Si NW Synthesis, Smaller Critical Diameter, and Lower Free Energy of [110]-Si NW. Figure 2a,b shows the dependencies of the Si NW critical diameter d_{cr}

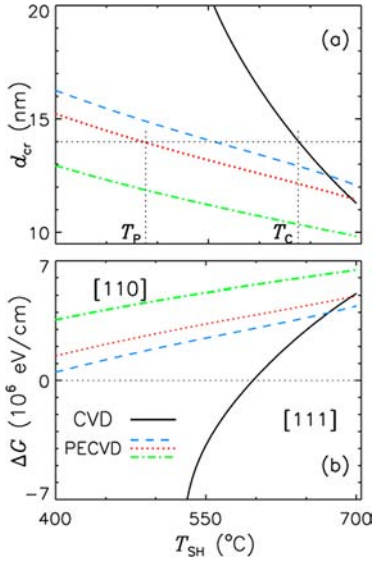

Figure 2. Numerical modeling results on the minimum possible Si NW diameter and the preferential growth along the [110] and [111] directions. (a) The critical Si NW diameter d and (b) the free energy difference (per unit length) for the formation of [111]- and [110]-oriented Si NWs (ΔG) are plotted as functions of the substrate holder temperature for T_e = 1.0 eV, T_i = 0.15 eV, P_{SiH} = 10 mTorr, and V_{DC} = −20 V. Here, the cases of both CVD (solid curve) and PECVD (dashed, dotted, and dash-dotted curves) are considered. Dashed, dotted, and dash-dotted curves correspond to $n_{e0} = 5 \times 10^{11}$, 10^{12}, and 5×10^{12} cm^{-3}, respectively. T_C and T_P represent the temperature conditions for the growth of [110] Si NWs with a diameter of 14 nm in CVD (C) and PECVD (P) cases, respectively.

(the minimum possible Si NW diameter) and the difference between the free energies (per unit length) of [111]- and [110]-oriented Si NWs on the substrate holder temperature T_{SH} in the CVD and PECVD processes at the same gas mixture and external heating conditions. From Figure 2a, it is clearly seen that, at almost all the temperatures, much thinner Si NW can nucleate and grow in PECVD compared to CVD. Moreover, the critical diameter in the CVD process becomes much larger as the temperature decreases, while it is smaller than the CNP diameter ($2r_{Au}$=20 nm) in the PECVD case. It is seen that the temperature for nucleation of a Si NWs with the specific diameter and orientation (d_{cr} = 14 nm and [110]) can be reduced significantly in the plasma-based synthesis, so that Si NW growth along the [110] direction is possible at very low temperatures, such as 400 °C, or even lower achieved experimentally.[20,22] Likewise, by changing the plasma-specific parameters, it is possible to provide the sufficient level of supersaturation by generating larger numbers of BUs on the

dx.doi.org/10.1021/ja3110279 | J. Am. Chem. Soc. 2013, 135, 1912−1918

CNP surface. In this way, one can almost completely diminish the impact of the GT effect even at temperatures as low as 300 °C (see Figure S2), which is almost impossible in an equivalent thermal CVD process.

These results clearly show that the plasma heating and more effective Si atom generation enhance the level of AuSi supersaturation in the Au CNP (thus diminishing the adverse GT effect)[14] due to collisions of the plasma ions with the exposed Au NP surface. These collisions lead to the localized release of much higher energy (due to unique hydrogen-plasma processes, such as ion bombardment, H^+/H neutralization/recombination, etc.),[33] and also to the ion-induced decomposition of hydrosilicon radicals. As a result, the bulk and surface fluxes of Si atoms (through the catalyst and over the surface, respectively) become stronger. This in turn leads to the larger driving force $\Delta\mu_{LS}$ for the nucleation of Si ML (defined as a difference between the chemical potentials in the liquid droplet and the Si ML). This enhancement overcomes the reduced supersaturation due to the GT effect and enables nucleation of a very small-diameter Si MLs. Because a smaller-diameter Si ML forms at the catalyst−Si substrate interface, the vapor−solid (NW lateral) interface, yet not fully formed, will play the most important role in the choice of the growth direction. Given that {111} and {100} planes surrounding a [110]-oriented Si NW[27] have a lower surface energy compared to {110} planes (surrounding a [111]-oriented Si NW), subsequent Si MLs are formed along the [110] direction when the plasma is used. This demonstrates the indirect effect of the plasma-enabled localized heating and the enhanced production of BUs (effectively controlled through the variation of the plasma process parameters) on the energy and relative importance of the vapor−solid interface. We emphasize that the significant NW diameter difference between the CVD and PECVD processes (deduced from our calculations) is supported by the experimental observations (see also SI).[20] More details about the effects of nanoscale plasma chemistry can be found in SI and section 2.4.

The smaller Si NW critical diameters (which become even smaller under stronger plasma exposure, see Figure 2a) in PECVD experiments compared to CVD, enable the plasma-assisted nucleation of very thin Si NWs, where the NW lateral surface energy determines the Si NW growth direction.[25,27] This has been quantified in Figure 2b, where it is clearly seen that the free energy difference (per unit length) between the [111] and [110] growth directions, ΔG (= $\Delta G^{[111]} - \Delta G^{[110]}$), is much larger in the PECVD compared to the CVD. In other words, the [110] orientation is the most favorable growth direction in the plasma synthesis of Si NWs, and this tendency is strengthened with increasing the intensity of the plasma exposure (for example, by increasing the plasma density n_{e0}) as can be seen in Figures 2b and S2. This is because with increasing the plasma density, the plasma sheath shrinks very significantly which in turn leads to stronger electric fields across the sheath. As a result, the flux of ions that impinge on the Au catalyst surface increases, thus a larger amount of energy is released on the catalyst surface. Hence, more BUs are produced through the ion-assisted reactions of Si atom generation. The resulting flow of BUs is driven into the heated catalyst, which results in a much faster supersaturation (in the AuSi alloy) and precipitation of a smaller stable Si ML. This triggers the Si NW growth along [110] direction; this minimum-energy growth determines the development of the Si [110] NW system.

The numerical results in Figures 2b and S2 are in a good agreement with much higher ratios of densities of the [110]- and [111]-oriented NWs in plasma-assisted Si NW growth experiments than in the CVD processes.[20,21] Moreover, for very thin Si NWs, the calculated increase of ΔG with increasing the temperature confirms the experimentally reported preferential nucleation of [110]-oriented NWs at high temperatures.[31,34] However, care should be taken not to overheat the samples and cause unnecessary coagulation of small CNPs into larger particles, which in turn gives rise to nucleation of thicker Si NWs predominantly oriented along the [111] direction.

2.3. Catalyst Radius and Gas Composition: High-Pressure Nucleation of Thinner [110] Si NWs. To illustrate the effects of the nanoscale plasma and neutral gas chemistries on the selectivity of the size and orientation of Si NWs, we have plotted the difference ΔG between the free energies (per unit length) of the [111]- and [110]-oriented Si NWs, as a function of the Au NP radius r_{Au} and the SiH_4 gas pressure P_{SiH}, see Figure 3a,b. From Figure 3a, one can observe that with

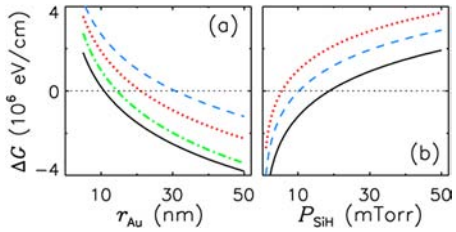

Figure 3. Effects of variations in the Au catalyst radius (a) and the silane gas pressure (b) on the difference between the free energies (per unit length) of [111]- and [110]-oriented Si NWs in CVD [solid curve in (a)] and PECVD [dashed, dotted, and dash-dotted curves in (a) and all curves in (b)]. Unless varied in the graphs, the set of default parameter is T_e = 1.0 eV, T_i = 0.15 eV, $n_{e0} = 5 \times 10^{11}$ cm^{-3}, P_{SiH} = 10 mTorr, and V_{DC} = −20 V for (a) and T_e = 1.0 eV, T_i = 0.15 eV, $n_{e0} = 5 \times 10^{11}$ cm^{-3}, r_{Au} = 10 nm, and V_{DC} = −20 V for (b). Solid and dashed curves in (a) correspond to T_{SH} = 600 °C, while the dotted and dash-dotted correspond T_{SH} = 550 and 500 °C. Solid, dashed, and dotted curves in (b) correspond to T_{SH} = 400, 450, and 500 °C, respectively.

decreasing r_{Au}, the energy difference ΔG tends to higher values indicating that the [110] growth direction would be favorable for thinner Si NWs. As mentioned above, this tendency is stronger at higher temperatures or under the plasma-based process conditions, when the Au catalyst heating and Si atom production are more effective, which improves the BU transport inside the nanoparticle. Consequently, a smaller stable Si ML is formed at the catalyst−substrate interface. This explains why the [110]-oriented Si NWs tend to grow in the ionized gas-based process. Meanwhile, a weaker tendency to the growth in the [110] direction at smaller r_{Au} suggests that the impact of the GT effect (which makes the Si atom transport less effective thereby reducing the saturation of Si atoms in AuSi alloy) is quite significant in thermal CVD.

On the other hand, this impact is much less significant under the plasma conditions when the required BUs are produced locally and more effectively, which gives rise to the nucleation of much smaller Si MLs (see Figure S3a) and eventually, much thinner NWs. The growth preference in the [110] direction at smaller CNP radii computed here is in a good agreement with numerous experiments on the nucleation and growth of various inorganic NWs.[17,18,26]

dx.doi.org/10.1021/ja3110279 | J. Am. Chem. Soc. 2013, 135, 1912−1918

The change of the free energy difference with the precursor gas pressure clearly reveals the very strong dependence of the Si NW growth orientation on this process parameter (see Figure 3b). It is seen that with increasing the precursor gas pressure P_{SiH}, the difference between the free energy (per unit length) for the [111] and [110] orientations becomes larger as the pressure increases. Therefore, Si NWs are more likely to grow along the [110] direction at higher precursor gas pressures. This can be understood by noting that at higher SiH_4 pressures more precursor molecules hit the Au catalyst surface and are thermally decomposed. As a result, much larger numbers of Si atoms are produced to diffuse through the CNP bulk and the surface into the catalyst. Consequently, the AuSi alloy inside smaller CNPs supersaturates and a much smaller stable Si ML can nucleate at the Si−Au interface (see Figure S3b).

This in turn leads to the growth of thin Si NWs along the [110] direction as a result of the thermodynamically favorable lower-energy faceting of [110]-oriented Si NWs. This evidence the role of SiH_3 radicals in the selection of the Si ML size and, hence, the surface energy of the vapor−solid interface. It is worth mentioning that the precursor pressure for this transition can be reduced to smaller values by increasing the temperature (see Figures 3b and S4b) and plasma-specific parameters (see Figure S5). The calculated changes in the energy difference ΔG with P_{SiH} explains the experimental observations of the predominant growth of [110]- and [111]-oriented NWs at high-pressure and the low-pressure conditions.[16,30,35,36]

2.4. Plasma Effects: Controlling the Size and Orientation of Si NWs. To further discuss the roles of the plasma-specific effects and give suggestions for improving the selectivity of the NW growth orientation, we have linked the plasma-specific parameters (the bulk plasma density n_0, the electron temperature T_e, and the substrate voltage V_{DC}), the Au NP radius r_{Au}, and the difference between the free energies of [111]- and [110]-oriented Si NW (ΔG). The three panels in Figure 4 show these links in a color-graded fashion. These results help identifying the plasma- and catalyst-parameter spaces, where, for example, the [110] orientation of Si NWs is more likely to happen under the given process conditions. This plot can also be used to control the NW size and orientation in a plasma-based synthesis process.

It is known that the plasma density n_0 (n_{e0}= n_{i0}= n_0 inside the plasma, where n_{e0} and n_{i0} are the electron and ion densities at the plasma-sheath edge) can quickly respond to the variation of the input power. This is why n_0 can be considered as an easy-to-control process parameter. When n_0 changes so does the plasma sheath width, which in turn determines the kinetic energies and fluxes of the ionic species. By adjusting the discharge power and hence the plasma density, the energy and fluxes of the ions impinging onto the catalyst surface can be optimized. Besides the plasma density, the electron temperature T_e and the substrate potential V_{DC} can also be used to control the dynamics of the plasma species and hence, the plasma-induced surface heating. For example, applying a DC bias is perhaps the easiest practical way for controlling the substrate potential, without significantly affecting the plasma discharge.

As the 3D color-graded contours in Figure 4 show, the combinations of the plasma and CNP parameters that are favorable for the preferential growth of the Si NWs along the [110] direction can be found in the color-graded zones (light- to dark-red colored areas) with the higher values of the plasma-specific parameters (n_0, T_e, and $|V_{DC}|$) and small Au CNP radii. Thus, when the plasma exposure is more intense (the plasma-specific parameters are higher), the size-selected growth of Si NWs is more probable along the [110] direction, which is considered the most promising Si NW orientation from the nanoelectronic and sensing applications points of view (see SI).[8,10,12] Here we stress that more intense fluxes of H^+ and SiH_3^+ ions onto the Au catalyst surface also contribute to the predominantly [110]-oriented NW growth. This gives rise to more effective localized heat release and Si atom production on the Au catalyst surface, which leads to more intense BU transport inside the catalyst bulk, faster Si atom supersaturation, and consequently, the formation of Si MLs along the [110] direction.

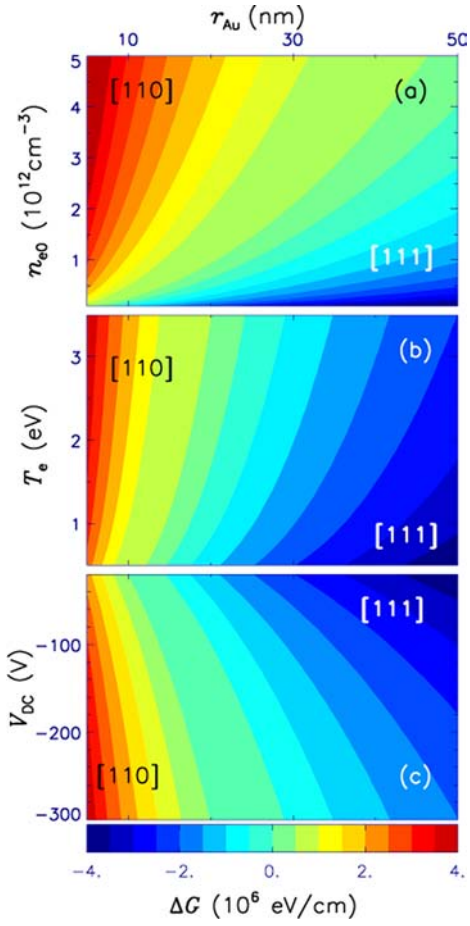

Figure 4. Link in a 3D parameter space between the plasma parameters [(a) plasma density n_{e0}; (b) electron temperature T_e; and (c) substrate voltage V_{DC}], Au catalyst radius r_{Au}, and free energy difference (per unit length) ΔG (between the growth of Si NWs along the [111] and [110] directions) in the plasma-based Si NW synthesis. Unless varied in any particular plot, the default set of parameters is T_{SH} = 500 °C, T_e = 1.0 eV, T_i = 0.15 eV, n_{e0} = 5 × 10^{11} cm^{-3}, P_{SiH} = 10 mTorr, and V_{DC} = −20 V. The colored bottom bar indicates the parameter regions appropriate for the growth of the Si NWs along the [111] and [110] directions.

The transition from the [111] to the [110] orientation in the Si NW growth due to the increases of the plasma-specific parameters can be explained by noting that all these variations lead to stronger fluxes of the energetic ions colliding with the catalyst surface. This happens due to larger kinetic energy gains after the ions transverse a thicker sheath[14,32,33] or when the surface density of the ion species is higher. This in turn leads to the release of larger amounts of heat on the catalyst surface. This heat helps overcoming the barriers for the SiH_4 thermal

dx.doi.org/10.1021/ja3110279 | J. Am. Chem. Soc. 2013, 135, 1912−1918

dissociation as well as leads to the production of larger amounts of Si atoms via ion-induced dissociation of precursor molecules and SiH^+_4 ion decomposition. Consequently, the CNP surface becomes hotter, and the number of Si atoms diffusing into the CNP bulk increases. As a result, the driving force (chemical potential difference) for nucleation increases, while the GT effect becomes negligible. In this case, smaller stable Si MLs can nucleate at the substrate−CNP interface, and hence much thinner Si NWs can grow. The energy of the Si NW-vapor surface is the determining thermodynamic factor at high Si NW surface-to-volume ratios. Hence, predominant growth of [110] Si NWs with a lower lateral surface energy can proceed under such plasma conditions. In this case, larger CNPs may still remain unsaturated.

This conclusion has been evidenced experimentally by carrying the Si NW growth under three different conditions: (1) only SiH_4 gas-based thermal growth; (2) SiH_4 plasma generation; and (3) first a short plasma stimulation followed by thermal growth, all for the same growth times.[20] The results showed that the density of [110]-directed thin Si NWs under condition 2 was the highest, followed by the densities in cases 3 and 1. This clearly shows the importance of the strength or the duration of the plasma exposure in controlling the orientation of the NWs in an array. These experimental results further confirm our results plotted in the 3D color-graded maps in Figure 4. The strong decrease of the density of [111]-oriented Si NWs observed in the plasma-assisted growth further evidence the improved selectivity toward the NW growth in the [110] direction in the plasma-based process compared to thermal CVD.

It is worth mentioning that the identified parameter ranges, representative to typical conditions of the plasma-based synthesis of NWs, can be used for controlling the plasma-process conditions to achieve large-area arrays with the high abundance of the NWs with the specific size and orientation appropriate for the targeted applications. This is particularly important when the NW arrays need to be fabricated on temperature-sensitive substrates, like plastic, as well as narrow distributions of sizes, and growth orientations are essential to enable the desired functionality in the envisaged applications. Therefore, the graphs in Figure 3 and 3D color-graded panels in Figure 4 (see also Figures S2, S4, and S5) make it possible to elaborate the most appropriate combination of the catalyst particle sizes, substrate temperature, precursor gas pressure, and the plasma parameters to produce the arrays of NWs with the desired sizes and orientations as well as using the minimum amounts of energy and atomic matter.

3. SUMMARY AND CONCLUSIONS

Our numerical model therefore explains the numerous experimental observations of the plasma-enabled transition of the Si NW growth to the most desired [110] direction at low temperatures.[20−22] These temperatures are much lower than the commonly used temperatures in thermal CVD,[17,26,34] where the undesired catalyst coagulation, deformation, etc. severely compromise the process outcomes. The results of this work are of practical importance since this transition between the growth orientations can be used to synthesize the arrays of [110]-oriented Si NWs tailored for specific applications.[8,10,12,13] This does not usually happen in low-temperature CVD experiments where the BU generation is less effective, while the impact of the GT effect is quite strong.[14] As a result, the critical diameters of stable Si NWs, below which the NW nucleation ceases, are quite large. In this case, when the surface energy of the catalyst−Si NW interface thermodynamically determines the growth direction, the {111} or {211} crystallographic planes with a lower surface energy (compared to that of the {110} plane) nucleate at the interface between the liquid droplet and the solid phase, thereby setting the NW growth along the [111] and [112] directions. In this work we have shown that this limitation can be removed, at all process temperatures, through the effects of the nanoscale reactive plasma chemistry, which provide high supersaturation levels, thus substantially diminishing the impact of the GT effect. This phenomenon is even more pronounced when the plasma effects become stronger and is in a very good agreement with the available experimental reports.[20,22]

We have also shown that the prevailing NW growth direction can be effectively controlled by precisely adjusting the plasma- and precursor gas-specific process parameters, such as the plasma density, electron temperature, applied substrate voltage, and precursor gas pressure. Therefore, based on these results we have also proposed a generic approach (based on precisely tailoring the process parameters) to control the size and orientation of the Si NWs, particularly, at the initial nucleation stage.

Finally, our multiscale, multiphase modeling is the first systematic thermokinetic study that explains numerous experimental reports on the possibility of the effective control of the NW size and the orientation in plasma-based chemical synthesis. Furthermore, it provides an exciting opportunity to customize the plasma conditions to eventually achieve truly energy- and matter-efficient fabrication of the arrays of inorganic NWs with the required size and crystallographic orientation. This ability is highly warranted by the rapidly emerging energy conversion, biosensing, and nanoelectronic applications that heavily rely on useful properties of such NWs.

4. MODELS AND COMPUTATIONAL METHODOLOGY

As mentioned in section 2.1, our multiscale, multiphase model includes the plasma sheath, ion/radical transport (module 1), neutral/ionized gas−surface interactions, heat transfer, building unit generation and surface/bulk diffusion (module 2, right inset in Figure 1) as well as catalyst saturation, Si ML nucleation (module 3, right inset in Figure 1 and Figure S1a) and growth along a specific directions modules (module 4, Figure 1b,c). Module 1 includes sets of equations that describe the transport of the selected neutral and charged species in the plasma sheath,[37] their energies and fluxes onto the surfaces of the substrate and CNPs. This module links the parameters of the plasma bulk and substrate bias to the parameters of heat transfer and building units generation and diffusion on/into the Au CNPs.

Module 2 includes mass and energy balance equations on the surface of Au CNPs which account for contributions from a large number of thermal and plasma-specific chemical reactions, such as, e.g., (see Figure 1 right inset) thermal dissociation (TD) of main radical species:

$$SiH_{3(surface)} \rightarrow Si_{(surface)} + H_{(surface)} + H_{2(sheath)}$$

ion-induced radical/molecular dissociation (IID):

$$SiH_3^+ + SiH_{3(surface)} \rightarrow Si_{(surface)} + H_{(surface)} + H_{2(sheath)} + SiH_3^+$$

dx.doi.org/10.1021/ja3110279 | J. Am. Chem. Soc. 2013, 135, 1912−1918

ion decomposition (ID):

$$SiH_3^+ \rightarrow Si_{(surface)} + H_{(surface)} + H_{2(sheath)}$$

hydrogen atom recombination:[14,32]

$$H_{(surface)} + H_{(sheath)} \rightarrow H_{2(sheath)} + 4.5eV$$

and hydrogen ion neutralization:[14,32]

$$H_{(surface)} + H^+_{(sheath)} \rightarrow H_{2(sheath)} + 13.2eV$$

on the CNP surface of temperature T_{Au}, which is calculated as a function of the substrate holder temperature T_{SH} . Surface (SD) and bulk (BD) diffusion of Si atoms are described using the input from Module 1 and the radical/atom production/loss equations and taking into account the plasma-affected temperature of the Au CNP. The heat balance equations, complemented with appropriate boundary conditions, are used to compute T_{Au} and its difference from T_{SH}.

Module 3 takes into account the possible Si atom fluxes into/out of a Au CNP and is used to calculate temperature- and size-dependent solubility of Si atoms in the Au CNP, which this yields finding the difference between the chemical potentials within the CNP and its surface; this difference is the driving force for the Si ML nucleation at the CNP−substrate interface. By obtaining the chemical potential modified by the size-dependent GT effect,[14] the (minimum energy and) possible minimum diameter for stable Si ML formation can be computed and is intimately related to surface and neutral/plasma-process parameters used as input in Module 1. Finally, the difference between the free energies (per unit length) of [111]- and [110]-oriented Si NWs is obtained as a function of the critical diameter. For more detailed description, main assumptions, and limitations of the specific modules within our model please refer to the SI and our previous publications.[14,32,33]

■ ASSOCIATED CONTENT

Ⓢ Supporting Information

Theoretical and experimental reports on the importance of [110]-oriented Si NWs, main equations of the model and the description of calculation procedures, additional results on the effects of variations of the plasma-specific parameters on the orientation transition, and their relevance to the experimental results. This material is available free of charge via the Internet at http://pubs.acs.org.

■ AUTHOR INFORMATION

Corresponding Author

Kostya.Ostrikov@csiro.au

Author Contributions

†H.M. and K.O. contributed equally to this work.

Notes

The authors declare no competing financial interest.

■ ACKNOWLEDGMENTS

This work was partially supported by the Australian Research Council and CSIRO's OCE Science Leadership Program. H.M. acknowledges supports by the University of Sydney International Scholarship and CSIRO OCE top-up scholarship.

■ REFERENCES

(1) Meyyappan, M.; Sunkara, M. K. *Inorganic NWs: applications, properties, and characterization*; CRC Press: New York, 2010.
(2) Sharma, S.; Sunkara, M. K. *J. Am. Chem. Soc.* **2002**, *124*, 12288.
(3) Shieh, J.; Hou, F. J.; Chen, Y. C.; Chen, H. M.; Yang, S. P.; Cheng, C. C.; Chen, H. L. *Adv. Mater.* **2010**, *22*, 597.
(4) Cvelbar, U.; Chen, Z. Q.; Sunkara, M. K.; Mozetic, M. *Small* **2008**, *4*, 1610.
(5) Qin, Y.; Wang, X. D.; Wang, Z. L. *Nature* **2008**, *451*, 809.
(6) Huang, M. H.; Mao, S.; Feick, H.; Yan, H.; Wu, Y.; Kind, H.; Weber, E.; Russo, R.; Yang, P. *Science* **2001**, *292*, 1897.
(7) Fujiwara, A.; Inokawa, H.; Yamazaki, K.; Namatsu, H.; Takahashi, Y.; Zimmerman, N. M.; Martin, S. B. *Appl. Phys. Lett.* **2006**, *88*, 053121.
(8) Buin, A. K.; Verma, A.; Svizhenko, A.; Anantram, M. P. *Nano Lett.* **2008**, *8*, 760.
(9) Khalilov, U.; Pourtois, G.; van Duin, A. C. T.; Neyts, E. C. *Chem. Mater.* **2012**, *24*, 2141.
(10) Neophytou, N.; Klimeck, G. *Nano Lett.* **2009**, *9*, 623.
(11) Fagas, G.; Greer, J. C. *Nano Lett.* **2009**, *9*, 1856.
(12) Murphy-Armando, F.; Fagas, G.; Greer, J. C. *Nano Lett.* **2010**, *10*, 869.
(13) Ma, D. D. D.; Lee, C. S.; Au, F. C. K.; Tong, S. Y.; Lee, S. T. *Science* **2003**, *21*, 1874.
(14) Ostrikov, K.; Mehdipour, H. *Appl. Phys. Lett.* **2011**, *98*, 033104.
(15) Westwater, J.; Gosain, D. P.; Tomiya, S.; Usui, S.; Ruda, H. *J. Vac. Sci. Technol., B* **1997**, *15*, 554.
(16) Ge, S.; Jiang, K.; Lu, X.; Chen, Y.; Wang, R.; Fan, S. *Adv. Mater.* **2005**, *17* (1), 56.
(17) Wu, Y.; Cui, Y.; Huynh, L.; Barrelet, C. J.; Bell, D. C.; Lieber, C. M. *Nano Lett.* **2004**, *4*, 433.
(18) Madras, P.; Dailey, E.; Drucker, J. *Nano Lett.* **2009**, *9*, 3826.
(19) Wen, C.-Y.; Reuter, M. C.; Tersoff, J.; Stach, E. A.; Ross, F. M. *Nano Lett.* **2010**, *10*, 514.
(20) Aella, P.; Ingole, S.; Petuskey, W. T.; Picraux, S. T. *Adv. Mater.* **2007**, *19*, 2603.
(21) Hofmann, S.; Ducati, C.; Neill, R. J.; Piscanec, S.; Ferrari, A. C.; Geng, J.; Dunin-Borkowski, R. E.; Robertson, J. *J. Appl. Phys.* **2003**, *94*, 6005.
(22) Yu, L.; Alet, P. -J.; Picardi, G.; Maurin, I.; Cabarrocas, P. R. *Nanotechnology* **2008**, *19*, 485605.
(23) Neyts, E. C.; van Duin, A. C. T.; Bogaerts, A. *J. Am. Chem. Soc.* **2012**, *134*, 1256.
(24) Mariotti, D.; Sankaran, R. M. J. *Phys. D* **2010**, *43*, 323001.
(25) Vasilev, K.; Sah, V.; Anselme, K.; Ndi, C.; Mateescu, M.; Dollmann, B.; Martinek, P.; Ys, H.; Ploux, L.; Griesser, H. J. *Nano Lett.* **2010**, *10*, 202.
(26) Schmidt, V.; Senz, S.; Gosele, U. *Nano Lett.* **2005**, *5*, 931.
(27) Hanrath, T.; Korgel, B. A. *Small* **2005**, *1*, 717.
(28) Glas, F.; Harmand, J. -C.; Patriarche, G. *Phys. Rev. Lett.* **2007**, *99*, 146101.
(29) Cui, Y.; Lauhon, L. J.; Gudiksen, M. S.; Wang, J.; Lieber, C. M. *Appl. Phys. Lett.* **2001**, *78*, 2214.
(30) Holmes, J. D.; Johnston, K. P.; Doty, R. C.; Korge, B. A. *Science* **2000**, *287*, 1471.
(31) Cai, Y.; Chan, S. K.; Sou, I. K.; Chan, Y. F.; Su, D. S.; Wang, N. *Small* **2007**, *3*, 111.
(32) Ostrikov, K.; Mehdipour, H. *ACS Nano* **2011**, *5*, 8372.
(33) Ostrikov, K.; Mehdipour, H. *J. Am. Chem. Soc.* **2012**, *134*, 4303.
(34) Peng, H. Y.; Wang, N.; Zhou, X. T.; Zheng, Y. F.; Lee, C. S.; Lee, S. T. *Chem. Phys. Lett.* **2002**, *359*, 241.
(35) Jagannathan, H.; Deal, M.; Nishi, Y.; Woodruff, J.; Chidsey, C.; McIntyre, P. C. *J. Appl. Phys.* **2006**, *100*, 024318.
(36) Irrera, A.; Pecora, E. F.; Priolo, F. *Nanotechnology* **2009**, *20*, 135601.
(37) Keidar, M.; Beilis, I. I. *Appl. Phys. Lett.* **2009**, *94*, 191501.